Compare Results

Total Changes

553

Content

257 Replacements

120 Insertions

148 Deletions

Styling and Annotations

9 Styling

19 Annotations

Go to First Change (page 1)

Added value of site load measurements in probabilistic lifetime extension: a Lillgrund case study

Shadan Mozafari[1,*], Jennifer Marie Rinker[1], Paul Veers[2], and Katherine Dykes[1]

[1]Department of Wind Energy, Technical University of Denmark, Roskilde, Denmark
[2]National Renewable Energy Laboratory (NREL), Golden, CO, USA.

Correspondence: Shadan Mozafari (Shad.mzf@gmail.com)

Abstract.

Estimating site-specific fatigue reliability of wind turbines is an integral part of probabilistic lifetime extension assessment. Different approaches are possible for such estimation based on different scenarios of data availability.

This study presents a probabilistic lifetime extension assessment under two different data availability scenarios: with and without site load/displacement measurements at the blade root. The comparison highlights the benefits of incorporating site load measurements. Additionally, we address two common challenges in these scenarios: the temporal extrapolation of mid-term data and the applicability of the Frandsen model—used for estimating waked turbulence—in complex and mixed wake conditions. The case study wind turbine is a Siemens 2.3MW in the Lillgrund wind farm, located in the Øresund strait between Denmark and Sweden. The turbine is extensively instrumented, with five years of data available from its Supervisory Control and Data Acquisition (SCADA) system.

Results indicate that the Frandsen model underestimates turbulence at below-rated mean wind speeds and overestimates it at above-rated mean wind speeds, though it remains conservative concerning fatigue loads and reliability. Furthermore, a site specific assessment using strain gauge measurements results in a 33% higher annual reliability index after 35 years, compared to the scenario relying on ambient environmental conditions and the Frandsen model. Finally, the sensitivity of fatigue reliability to load uncertainty is negligible when using load measurements, but relatively high when relying on the Frandsen model.

keywords: Frandsen model, Lifetime extension, Digital twin, Fatigue reliability, Wind farm wakes, Statistical extrapolation, Wind turbines

1 Introduction

Exposure of wind turbines to the wakes within a wind farm increases fatigue loads they experience Kim et al. (2015); Lee et al. (2012); Frandsen (2007) The design assumptions in IEC 61400-1 standard are often conservative enough to seek an extension of the operation time even after experiencing the high fatigue loads caused by wakes in the wind farms. Extending the operation time above the design service life (typically 20-25 years), in cases where maintaining safety is possible, is environmentally beneficial and can reduce the levelized cost of energy Dimitrov and Natarajan (2020); Natarajan et al. (2020).

When it comes to lifetime extension of wind turbines in a wind farm, one must re assess the service lifetime by replacing the design assumptions with the conditions experienced in the site. In such re-assessments, normally, fatigue is the main subject of interest because of its direct functionality of time. The information about lifetime in site can be gathered in different manners based on data availability. Some of the common scenarios are as below:

1. In case only free-stream turbulence measurement is available, one can estimate the waked turbulence in each turbine's location using simplified models like Frandsen Frandsen (2007); Frandsen and Madsen (2003), suggested by IEC 61400-1 (2019) for site suitability checks. The corresponding estimations are then used to perform aero-elastic simulations. Site-specific lifetime can be estimated using the resulting fatigue loads.

2. The turbulence measurements in the turbine's specific location might be available. In such scenario, one can use the measurements as inputs to the aeroelastic simulations and perform fatigue assessments. The time at which fatigue reliability reaches the target level can then be derived.

3. In some cases, the structural response (load/displacement) measurements are available for a limited duration of the lifetime in a specific hotspot. In case Supervisory Control and Data Acquisition (SCADA) also exist, one can form a digital twin for deriving the loads in other components/locations. On the other hand, direct utilization of the measurement data for assessing lifetime extension is also an option. However, the later involves challenges like spatial and temporal extrapolations.

Often the structural response measurements in the site are owned by the turbine manufacturer and are not accessible for the wind farm owner/developer. In addition, the measurements are not gathered for a long time or in many locations. The purpose of the current research is to showcase the differences of lifetime extension assessment in different scenarios (with and without load/displacement measurements) using a case study wind turbine for which all the above-mentioned scenarios are feasible. Additionally, the study tackles two common challenges in scenarios with and without structural response measurements. First, it addresses the question of performance of the Frandsen model—as a simplified approach for estimating enhanced turbulence due to wakes— in a compact wind farm layout. Second, we present a method for statistical extrapolation of mid-term strain gauge measurements for estimating long-term fatigue loads.

The Frandsen model involves simplified assumptions, and, thus, has some limitations. Bayo and Parro (2015) and Argyle et al. (2018) mention examples of limitation such as providing no prescription for the wake interaction from different wind turbines and the possibility of the model being under-conservative when the farm highly impacts the mean wind speed. Therefore, in wind farms with compact/irregular arrangements, ensuring the performance of the Frandsen model for conservative site-suitability checks is crucial. Despite all the studies on the performance check of the Frandsen model, the performance in the high-mixed wake conditions due to small spacing and irregular layouts has not been studied. We compare Frandsen estimations to the measured turbulence in the site to investigate the difference of estimated turbulence in different waked scenarios in the Lillgrund wind farm as an example of compact layout (small spacing between the wind turbines).

Another challenge for assessing site-specific assessment of the lifetime is data limitation and extrapolating the measurements to longer periods of time to assess the fatigue. How to determine the turbine-specific fatigue damage accumulated throughout

the operation time based on such limitation is still an important question. The answer is especially important for the offshore cases due to the high scatter of environmental data in offshore conditions. Some studies, including Amiri et al. (2019); Ziegler and Muskulus (2016), perform the lifetime extension assessment by assuming a linear damage increase through time. Such an approach can introduce errors in the estimations when the available data are insufficient to estimate the damage equivalent load (DEL) accurately. Although DEL is an averaged variable and thus is more robust to individual occurrences Mozafari et al. (2023b), it can still vary in different lengths of data for the components with high fatigue exponents. The results of Mozafari et al. (2023a) illustrate that the conventional approach of assuming the constant DEL, i.e., linear damage increase through time, can introduce bias in the long-term fatigue damage assessment in the case of the blade due to the composite's high fatigue exponent. Some researches like Dimitrov and Natarajan (2019); Natarajan et al. (2020) have used machine learning techniques and methods like Monte-Carlo simulations to generate long-term fatigue loads using mid-term measurements. Some other studies like Ling et al. (2011); Hübler et al. (2018); Natarajan (2022) use stochastic methods to anticipate long-term data based on mid-term measurements. Despite different statistical approaches and the guidelines given in IEC 61400-1 (2019), the best way to statistically extrapolate fatigue loads remains elusive.

We assess the possibility of extending the lifetime for 10 years for the blades of a wind turbine at the edge of the Lillgrund wind farm while maintaining acceptable safety margins. The case-study wind turbine is exposed to both non-waked and different scenarios of waked streams. First, using the available SCADA data, we study the performance of the Frandsen model in the safe estimation of the loads in the case study wind farm. We bin the different wake scenarios around the case study wind turbine for a more detailed assessment of Frandsen model turbulence estimations. The study uses the Gamma mixture model to extrapolate mid-term DEL data based on 10-minute strain measurements in the blade root to a 30-year lifetime. In addition, we investigate the relative importance of the loads, material fatigue strength, and damage accumulation rule in fatigue reliability estimation in different scenarios. Awareness about the effect of different sources of uncertainty on the assessment of lifetime extension is valuable. The procedure for anticipation of the probability of the DEL through lifetime will help the stakeholders and wind farm owners to get a better assessment of the fatigue damage in cases where strain gauge measurements are not available or are only available for a short span of the turbine's lifetime. To make the life extension results interesting for this particular example, the material properties are calibrated such that a target reliability index of 3.3 IEC 61400-1 (2019) is reached after 25 years based on design class (as using the recommended safety factors from the standard would result). Thus, although the comparisons of the reliability levels are correct, the magnitudes are not.

In the next sections, first, we present the methods and models we use for modeling and reliability assessment (Sect. 2). Then we present the results and corresponding discussions of the Frandsen performance check and lifetime extension assessments in Sect. 3. Finally, in Sect. 4, we present the conclusions of both studies and suggestions for future studies.

2 Methodology

First, we introduce the case study wind turbine and the corresponding wind farm in Sect. 2.1 and Sect. 2.2, respectively. Then, in Sect. 2.3, we present the setup and features of the aeroelastic simulations and site measurements. In addition, we introduce

the methods we use for assessing and filtering data for the current study. Finally, in Sect. 2.4, we introduce the mathematical formulas and the procedures we use for post-processing the simulation results and measurements.

2.1 The case study wind turbine

The wind turbine under study in the current research is SWT-2.3-93, manufactured by what is now Siemens Gamesa Renewable Energy (SGRE). The turbine has a 92.6-meter rotor diameter, a hub height of 65m, and a rated power of 2.3 MW. The cut-in and cut-out mean wind speeds are 3 m/s and 25 m/s, respectively, reaching the nominal power at approximately 12-13 m/s. The turbine belongs to class 1A based on the IEC 61400-1 standard's classification.

2.2 The case study wind farm

The strain-gauge and environmental measurements belong to one of the turbines in the edge of the Lillgrund offshore wind farm. Lillgrund wind farm is located about 10 km off the coast of Sweden in the Öresund region and consists of 48 Siemens SWT-2.3 93 wind turbines (total capacity of 110 MW). The turbines are arranged as shown in Fig. 1. The circles in Fig. 1 represent different turbines, and the red circle is the case study wind turbine, denoted as C08 (row c and column 8). We bin the wind directions around the case study wind turbine to roughly distinguish between different wake conditions. The binning facilitates assessing the performance of the Frandsen model and IEC NTM assumptions in characterizing turbulence in different wake scenarios. The dashed lines in Fig. 1 show the bins. For the rest of the study, we refer to the wind direction bins as 'wind bins' for simplicity.

As Fig. 1 illustrates, wind bin 1 accounts for non-waked conditions. In wind bins 2, 3, and 7, the stream is mainly passing by a single turbine, with bin 3 representing a relatively long distance between the turbine generating the wake and the C08 wind turbine. Wind bin 5 is an intense condition, with the case study turbine being very deep in the row and a very short distance between the closest wind turbine (4.3D). Bin 4 is a similar arrangement of a single row with a relatively long distance, and bin 6 is a mixed-waked flow condition. One should note that the binning and the corresponding conditions described are rough and are only used for general comparison.

2.3 Measurement data and aeroelastic simulations

In the present study, we use SCADA and 10-minute DEL evaluations extracted from a strain gauge installed on the blade root. The data represent long duration measurements over a span of 5 years in the Lillgrund wind farm. We also perform three groups of aeroelastic simulations in HAWC2 software Larsen and Hansen (2007): Group 1 based on IEC 61400-1 design requirements for wind turbine class A, Group 2 based on Frandsen's effective turbulence model (model explained in 2.4), and Group 3 based on site SCADA measurements in the non-waked wind directions for validation of the wind turbine model. In the following, first, we introduce the available measurement data (from the strain gauge and SCADA). Then, we present the specifications of the three groups of aeroelastic simulations.
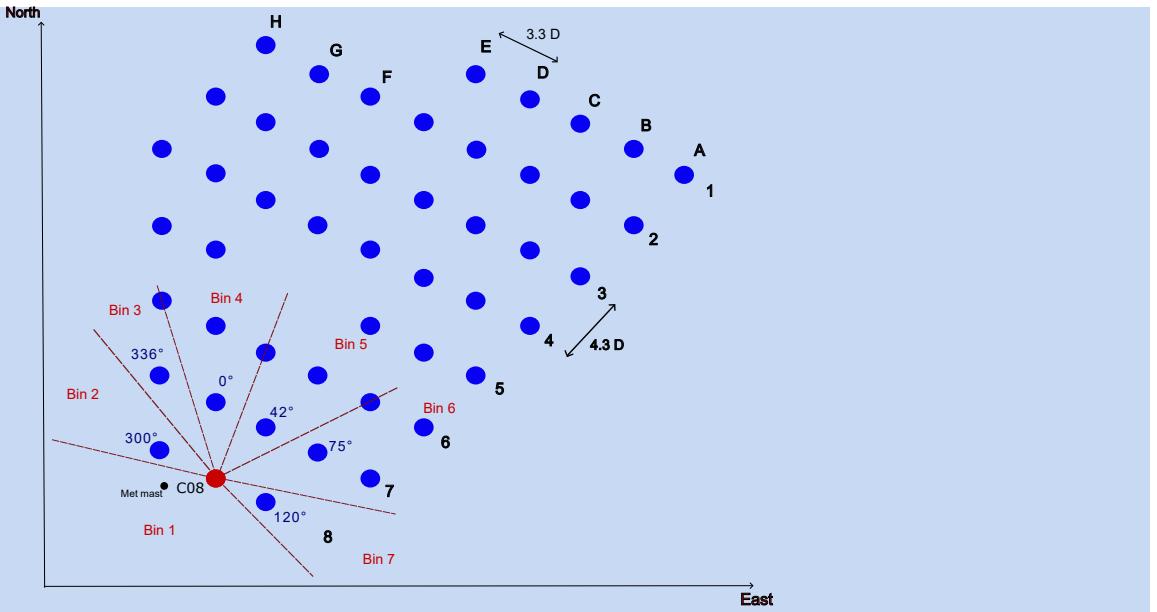
Figure 1. Arrangement of the wind turbines in the Lillgrund wind farm and the wind direction bins around the turbine C08 used in the current study

2.3.1 Measurement data

The available data are an integration of strain gauge data and SCADA data, including sensor measurements of wind speed, wind direction, power production, and rotor speed. The mean and standard deviation of wind are derived based on an anemometer installed on a tower very close to the case study wind turbine (black dot in Fig. 1). The meteorological mast is placed on a pole on top of the tower at the height of 65 meters (for more information see Bergström, H. (2009)). In addition, the strain gauge is installed at 1.5 m away from the blade root. All data are measured in time intervals of ten minutes during years 2008 to 2012. The strain gauge measurements are transformed into 10-minute DELs using the Palmgren-Miner approach, considering Wöhler exponent equal to ten for the composite structure of the blade. The measurement campaign has been running over 5 years but not continuously. The data covers about two years in terms of duration length. It includes different timings in the last 3 months of 2008 and all the months in 2009, 2010, 2011 and 2012. Thus, some data with a return period of 5 years are included among the measurements. Although the non-operational conditions should also be considered for fatigue assessments, in the current study, we only focus on normal operating conditions in the simulations (DLC 1.2 in the IEC standard). We use the provided DEL data to estimate the site-specific fatigue loads for the comparison study after filtration. We use the power curve of the turbine and utilize the data from SCADA, including mean wind speed, mean rotor speed, and the mean power production for the same points of time to exclude the corresponding DEL data. Thus, the wrong measurements and the ones that do not

represent the operational conditions are omitted (Fig. C1 in the appendix shows the power curve after such filtration). A total of 88031 data points remain after the filtration.

Table 1 shows the normalized number of data available in different wind direction bins around the C08 wind turbine (see the bins in Table 1) after filtration. In addition, table 1 shows the probability of occurrence of each bin based on the wind rose of the site Vitulli et al. (2019).

Table 1. Binning of wind directions and their corresponding probability in the Lillgrund wind farm site based on Vitulli et al. (2019)

Bin number	Wind direction bounds (degrees)	Probability (%)	Normalized number of available data
1	135-285 (non-waked)	55.5	0.5656
2	285-315	9.6	0.0741
3	315-345	5.0	0.0715
4	345-360, 0-15	5.4	0.0298
5	15-60	6.9	0.0623
6	60-105	9.3	0.1261
7	105-135	8.3	0.0851

As Table 1 illustrates, the available data after filtration do not fully cover the wind direction probabilities. This is partly because in some heavily waked conditions, the turbine has been shut down and partly because of the short duration of the data gathering. In the current work, we keep the mentioned observation in mind as a limitation. Thus, we proceed with assessing all DEL data together in fitting, extrapolation, and bootstrapping the samples. Fig. C3 (in appendix) shows the separate analysis of the DEL data in each wind direction bin. The analysis shows the rank of each wind bin in terms of the highest DEL observation and expectations. This analysis should be considered when accounting for fatigue assessments in each bin for more accurate assessments. However, as mentioned, in the current study, we estimate the damage accumulations based on assessment of the gross data. This limitation is discussed further in Sect. 4. The wind standard deviation (turbulence) data are used directly for fitting of the corresponding probability distributions in the turbine's location. In the current case, different distributions best describing the turbulence in each wind speed in the free stream is used. However, we do not present the details of those fits to be concise. We sample from the distributions and use them as input for aeroelastic simulations in the second part of the study (see Sect. 2.3.2).

2.3.2 Aeroelastic simulations

The current work includes three main simulation groups. Group 1 is based on inputs from IEC 61400-1 IEC 61400-1 (2005) requirements for design. Group 2 is based on the IEC 61400-1 recommendation for site suitability check, i.e., the Frandsen model. Group 3 is based on the site-specific inputs in terms of turbulence and wind shear exponent from the free stream (wind bin 1 in Fig. 1). The third group of simulations is only used for validation of the HAWC2 turbine model. The results of the validation checks are provided in the appendix.

Groups 1 and 2 have 11 mean wind speed bins (from 4m/s up to 24m/s with 2m/s intervals). Group 3 only includes the mean

wind speeds up to 20 m/s as the number of data points and probability of occurrence for the higher mean wind speeds are very low. The two first groups of simulations have one representative turbulence level in each mean wind speed bin. This level equals the 90% quantile value in group 1 and the Frandsen waked turbulence level in group 2 (more details are provided in the next section).

We consider 100 seeds for each wind condition to account for the variability of the wind Mozafari et al. (2023b) and have enough data for fitting distributions to the resulted DELs. The third group includes 20 samples from the site-specific turbulence standard deviation distribution in each mean wind speed in the free stream directions (wind bin 1). In this group, having nine mean wind speeds in the related wind directions, and 100 turbulence seeds for each turbulence level resulted in a total number of 22000 simulations of 10min duration for the site-specific aeroelastic simulations (group 3). Considering a lognormal wind profile in all simulations, we consider the shear exponent equal to 0.2 in the first two groups and equal to 0.1 in group 3 as an estimation for shear exponent in smooth terrain (open water)Yan et al. (2022). This value is also close to the Lidar measurements in the site Liew et al. (2023). We use the Mann turbulence model Mann (1998) to generate the simulation turbulence boxes. The boxes contain 8192 evaluation points alongside the wind direction for higher resolution and 32 points in the other two directions. Table 2 shows the specifications of each group of aeroelastic simulations.

Table 2. Specifications of wind modeling in three groups of Hawc2 simulations corresponding to three study cases

Parameter	Group 1	Group 2	Group 3
Turbulence in each mean wind speed	90% quantile in NTM	Frandsen's effective turbulence	Ambient turbulence distribution
Reference turbulence intensity	0.16	0.11	-
Turbulence levels in each MWS bin	1		20
Wind shear coefficient	0.1	0.2	
Realizations per wind condition	100		
Turbulence model	Mann		
Cut-in mean wind speed (m/s)	3		
Cut-out mean wind speed (m/s)	25		
Rated wind speed (m/s)	11.4		
Size of wind speed bins (m/s)	2		
Yaw angle (degrees)	0		
Mann box grids along the wind	8192		
Mann box grids in other dimensions	32		
Simulation length (sec.)	700		
Transient time (sec.)	100		
Time steps of the simulations (sec.)	0.01		

It shall be noted that group 1 is based on Edition 1 of the IEC standard and in case a full Lognormal or Weibull distribution are used (as in Editions 3 and 4, respectively), the results of the study differ (See Mozafari et al. (2024) for differences).

The following section includes the mathematical relations and procedures used in the study.

2.4 Mathematical formulations

In the current section, first, we introduce the wind characteristics, and then we briefly present the relations for fatigue load assessment plus methods for the reliability and importance ranks. Finally, we explain the procedure for forming the database for statistical extrapolation of DEL measurements via bootstrapping.

2.4.1 Probabilistic modelling of wind

In the current study, we only observe two random parameters of the wind field: mean wind speed and the wind speeds' standard deviation (turbulence). We consider the rest of the parameters as constants in the simulations. Following the IEC standard IEC 61400-1 (2019), we assume the distribution of the mean wind speed at hub height to be Rayleigh for both cases of design-level assessment and site-suitability check (the Frandsen model). In both these cases, the mean wind speed in the waked area is assumed to be the same as the free stream. In the case of site-specific assessment in non-waked conditions, we assume the same distribution as it complies with reality on the site. In the case of design-based assessment, we use 90% quantile of the lognormal distribution as suggested by the Normal Turbulence Model in IEC 61400-1 (2005) as the representative turbulence. Equation 1 presents this level.

$$\sigma_{rep.design} = I_{ref}(0.75v_{hub} + 5.6) \tag{1}$$

In Eq. 1, I_{ref} is the reference turbulence intensity equal to 0.16 for the standard class 1 wind turbines (the current case study). In addition, V_{hub} is the hub height wind speed.

In the Frandsen model, the free stream standard deviation is assumed to be the 90% quantile of a normal distribution Argyle et al. (2018). In the waked conditions, the turbulence is described as a function of the thrust coefficient and the normalized distance of the closest wind turbine. Equation 2 and Eq. 3 present the free stream standard deviation formulations and enhanced turbulence due to wakes in the Frandsen model.

$$\sigma_{rep.Frandsen} = \mu_\sigma + 1.28 * \sigma_\sigma \tag{2}$$

In Eq. (2), σ is the turbulence standard deviation (turbulence) of the free stream wind (ambient flow) considered as a random variable. In addition, μ_σ and σ_σ refer to the mean and standard deviation of the turbulence, respectively.

$$T_{waked}(\theta) = \sqrt{\frac{v_{hub}^2}{\left(1.5 + 0.8\left(\frac{di(\theta)}{\sqrt{C_T}}\right)\right)^2} + \sigma_{rep.Frandsen}^2} \tag{3}$$

In Eq. 3, θ is the (wind) direction in which the waked turbulence is estimated, $d_i(\theta)$ is the distance of the closed turbine in that direction and C_T is the characteristic value of the wind turbine thrust coefficient for the corresponding hub height wind velocity IEC 61400-1 (2019).We use the thrust coefficient data provided in Montavon et al. (2009) for the current study.

The Frandsen model's turbulence is the same in all wind directions (like in IEC design assessments). This independence from wind direction is obtained by effective turbulence. Equation 4 shows the effective turbulence used for site-suitability check IEC 61400-1 (2019).

$$T_{eff}(V_{hub}) = \left(\sum_{\theta=0}^{2\pi} P_\theta(V_{hub})(T_{waked}(\theta))^m \right)^{\frac{1}{m}} \tag{4}$$

In Eq. 4, $P_\theta(V_{hub}$ is the probability of occurrence of the hub height mean wind speed in each direction (θ), and m is the fatigue (wöhler) exponent Basquin (1910)[1].

2.4.2 DEL estimation

In the present research, we use the Basquin relation Basquin (1910) for modeling the fatigue resistance of the composite material and Palmgren–Miner (Miner's) rule Palmgren (1924); Miner (1945) for modeling the damage accumulation. These models describe the lifetime and damage as functions of stress, while the outputs of the aeroelastic simulations that we use are flapwise bending moments in the blade root. Since the location of the interest (the strain-gauge installation location) is close to the root and nearly circular, we use Eq. 5 to obtain the stresses based on the moment time series.

$$S_i = \frac{M_{x_i} \times c}{I_y} \tag{5}$$

In Equation 5, Mx_i is the moment corresponding to the stress level S_i. In the current study, the direction y corresponds to the global direction of the wind in the HAWC2 simulations. Thus, we consider moments in the perpendicular direction (Mx). In addition, the section parameters c and I_y are the radius (half of the chord) and the moment of inertia in the direction perpendicular to the moment's direction, respectively. The corresponding values are not mentioned here because of confidentiality.

Using rain flow counting Endo et al. (1967) of the moments in each 10-minute simulation and the models mentioned (Basquin and Palmgren–Miner), we estimate the 10-minute fatigue damage via Eq. 6.

$$D = \left(\frac{c}{I_y} \right)^m \sum_{i=1}^{Ns} \frac{n_i \times (M_{x_i})^m}{k} \tag{6}$$

In Eq. (6), N_S is the total number of cycles at the time frame considered for calculation of the damage. In addition, m is the fatigue exponent and k is the Basquin coefficient (see Basquin (1910)). Reformulation of the Eq. 6 using the concept of

---

[1]For further details and derivation of the equations 3 and 4, see Frandsen (2007) and IEC 61400-1 (2019).

damage equivalent load (DEL) (see Mozafari et al. (2023b) for more information) results in Eq. 7. We use this expression in the current study to simplify the comparisons.

$$D = \frac{Neq(DEL_{lifetime}^m)}{k}\left(\frac{c}{I}\right)^m \tag{7}$$

In Eq. (7), N_{eq} is the reference number of cycles. we set N_{eq} equal to 600 cycles corresponding to the average of 1Hz. Cyclic loading. In addition, $DEL_{lifetime}$ (The expected value of the fatigue damage equivalent load through lifetime)can be derived from 10-minute DEL estimations via Eq. 8.

$$DEL_{lifetime}^m = \sum_{\Theta=\Theta_L}^{\Theta_U} \sum_{V_\Theta=V_L}^{V_U} \sum_{T_{(\Theta,V)}=T_L}^{T_U} E[(DEL_{10min,\Theta})^m]\mathrm{P}(T,V|\Theta)\mathrm{P}(\Theta) \tag{8}$$

In Eq. (8), the parameters Θ_L and Θ_U, V_L, and V_U, as well as t_L and t_U, represent the lower bound and higher bound for mean wind speed and turbulence in each wind bin. Furthermore, $\mathrm{P}(T,V|\Theta)$ is the joint probability of the directional turbulence and mean wind speed bins conditioned on different direction bins. As we are considering the marginal probability of turbulence conditioned on the mean wind speed bin, and the probability of each mean wind speed conditioned on the direction, the joint probability equals the multiplication of the three conditional probabilities. In the case of assessments with constant turbulence in each mean wind speed (Frandsen effective and IEC representative turbulence characterization), the probability of the single turbulence level equals 1. In the case of group 3 simulations, we account for the probability distribution of turbulence in each wind speed bin, and the probability of the wind direction bin is set to 1 (as we only consider wind bin 1 for validation of the model). In measurement-based assessments, the DEL is derived based on the un-weighted average of DEL_{10min} assuming that the database is large enough to have the probabilities fairly accounted for automatically. In other words, the probability of the wind conditions is already embedded in forming the distribution of 10-minute DEL measurements. Equation 9 shows the relation between DEL_{10min} and $DEL_{lifetime}$ in case of n number of DEL_{10min} available.

$$DEL_{lifetime}^m = \sum_{i=1}^{n} \frac{(DEL_{10min_i})^m}{n} \tag{9}$$

In Eq. 9, in the case of DEL in one year, n would be the number of 10 minutes within the timeline of 1 year. If enough DEL_{10min} data are not available, one has two options: statistical extrapolation (as in the current study) or assuming that the same observations repeat during the longer times (For reference to the importance of statistical extrapolation in estimation of $DEL_{lifetime}$ please see Mozafari et al. (2023a) and Mozafari et al. (2023b)).

2.4.3 Forming the DEL database based on measurements and statistical extrapolation

For the site-specific (measurement-based) assessment of reliability, we need to obtain the distribution of the $\log(DEL_{lifetime})$ in each year to put in Eq. 14 to be able to estimate the annual reliability level up to year 30 using Eq. 16. We prepare the data

for such assessments for up to 30 years. To do so, we follow the below procedure:

1. Fitting a distribution to the 10-minute DEL measurements

2. Forming a database based on the distribution found in step 1 and extrapolating to 30-year return loads (Eq. 10 to 12)

3. Taking random 500 samples of size $365 \times 24 \times 6 \times N$ from the database with replacement; N accounting for the year number and repeating from year 1 to 30.

4. Calculating the mean of $(DEL_{10min})^m$ in each of the 500 samples and estimating the corresponding $DEL_{lifetime}$ based on Eq. 9.

5. Calculating the logarithm of all generated data and fitting probability distribution to the 500 realizations of $\log(DEL_{lifetime})$ in each year.

For forming the database (step 2 above), first, we find the probability of exceedance corresponding to 30-year return period using Eq. 10 and Eq. 11. The return load is the load that can happen once in a duration equal to the return period. The extrapolation is used to complete the tail of the DEL_{10min} distribution to account for highest values that might change the weighted mean value ($DEL_{lifetime}$) if included. These values can have high effect due to the high fatigue exponent of the composite (Mozafari et al. (2023b))

$$CDF(L_R) = \exp\left(\frac{-1}{T_{L_R}}\right) \tag{10}$$

$$Pr_{exc.}(L_R) = (1 - CDF(L_R)) \tag{11}$$

In Eq. 10 and Eq. 11, L_R accounts for the return load level, and T_{L_R} in Eq. 10 accounts for the ultimate time of interest for which the return load is estimated. Equation 10 is extracted from formula of probability of exceedance a threshold level (here the load with frequency of occurance of every 30 years) assuming a Poisson process for describing the peaks over threshold problem (for further information see de Oliveira JT (2013)). In the current case, the frequency of exceedance is $1/T_{L_R}$. It has to be noted that Eq. 10 is correct when T_{L_R} is relatively large (here, equal to the number of 10 minutes in 30 years). We set the time in terms of the number of 10 minutes because we consider the DEL to be the load, and in this case, each DEL is an occurrence of a 10-minute duration. The $Pr_{exc.}(L_R)$ in 11 is the probability of exceedance of such load, meaning the probability that a load higher than that level occurs. In the case of return loads, this probability is normally very low. We use the CDF corresponding to the return period, obtained from Eq. 10, to find the return load in our case. This load can be derived by finding the inverse CDF of the distribution of our 10-minute data (step 1 above). After finding the return load, we can find the number of occurrences of each DEL level in our database based on Eq. 12. In other words, first, the maximum loads with a certain reference return period are defined, and the frequency of lower loads is derived accordingly.

$$i = \frac{1}{\Pr(L_R)} \tag{12}$$

In Eq. 12, i is the number of occurrences of each 10-minute DEL level DEL_{10min} and $Pr(L_R)$ is the probability of occurrence of the return load based on the distribution of DEL_{10min}s (distribution in step 1 above). Equation 12 is based on the assumption that the probability density functions of DEL_{10min} remain the same when more observations are added to the tail through time. The more data involved in fitting the distribution of DEL_{10min}, the more accurate this assumption is.

2.4.4 Fatigue reliability estimation

Fatigue reliability assessment is performed to obtain an estimation of the probability of the survival of a structure. Equation 13 presents a mathematical representation of this concept.

$$R(t) = 1 - P_f(t) \tag{13}$$

In Eq. 13, $P_f(t)$ is the probability of failure at time t. Commonly, this problem is referred to with a function named limit state function $(g(x,t))$, and the safe region is where this function is positive. Thus, the probability of failure would be the probability of lying in a region in the space of random variables where the limit state function is negative or equal to zero. We fully follow the methods and procedures used in our previous work in Mozafari et al. (2024) for reliability estimation. Here, we present a brief introduction and the general approach. We recommend the reader to check Mozafari et al. (2024) for further details.

Following Miner's rule, failure can happen when damage is higher than a threshold level (commonly 1). This rule contains uncertainty due to simplified assumptions like linear damage accumulation without sequence effect. To account for the uncertainty in Miner's rule, we assume the threshold (Δ) as a random variable with a mean value equal to 1. Thus, the reliability being the probability of survival, would be the probability of damage being less than Δ. Equation 14 describes the limit state function considering DEL, K, and Δ as random inputs for the case of flapwise bending moments in the blade root with a circular cross-section and structural properties of I_y and c (moment of inertia and diameter, respectively). The time is omitted from Eq. 14 for simplicity with the assumption that all variables are referring to a certain time.

$$g(X) = \log(\Delta) - \log(N_{eq}) - m \times \log\left(\frac{c}{I_y}\right) + \log(k) - m \times \log(DEL_{lifetime}) \tag{14}$$

The parameters $log(N_{eq})$ and $m \times log(\frac{c}{I_y})$ in Eq. 14 are constants. Thus, the above equation consists of three random parameters:

- The linear damage accumulation model $(\log(\Delta))$

- Material Resistance $(\log(k))$

- Load ($\log(DEL_{lifetime})$)

We perform the probabilistic reliability assessment using first order reliability method (FORM) in the current work to find the probability that the function g in Eq. 14 can be positive (fatigue reliability). The same approach also provides the importance rank of the random variables (sensitivity of the reliability to each) and is used here (see Mozafari et al. (2024) for details and formulations). We use the reliability index (shown in Eq. 15) as a commonly used measure of structural reliability.

$$\beta = -\Phi^{-1}(P_f) \tag{15}$$

The operator Φ^{-1} shown in Eq. 15 corresponds to the inverse cumulative distribution function (CDF) of the standard normal distribution.

We consider $R = 10$ for fatigue properties (SN curve) of the composite Mikkelsen (2020). Although the variability of data is included as the CoV of such curve, a calibration is added at the end to set the mean value of material strength to a certain level at which target level of reliability is obtained at year 20.

To apply FORM analysis, first, we fit distributions to the estimations of $\log(DEL_{lifetime})$ calculated based on 10-minute simulations using Eq. (9) for the measurement-based assessment and Eq. (8) for the simulation-based scenarios. For modeling the uncertainty in the model and material properties in the current study, we gather information regards the distributions and statistical parameters from the literature. Table 3 shows this information plus the references for the coefficients of variation.

Table 3. Characteristics of the random variables

Variable	Distribution	Mean	Coefficient of Variation	Reference
$log(\Delta)$	Normal	-0.1116	0.31	Toft and Sørensen (2011); Toft et al. (2016)
$log(K)$	Normal	Calibrated ($\beta = 3.7$ at year 20)	0.528	Fraisse and Brøndsted (2017)
$log(DEL_{lifetime})$	GEV	Confidential	0.001	Sect. 3.2

Equation 16 and Eq. 17 present the formulations for calculating the probability of failure and reliability index at time t ($P_f(X,t)$ and $\beta(X,t)$, respectively) conditional on survival in the previous point of time ($t - \Delta t$) considering a time interval of Δt. The parameter X is a vector of all random variables (the above-mentioned parameters for the current case study). For further information regarding derivation of Eq. 16 and Eq. 17, see Faber, M. H. (2012).

$$\Delta P_f(X,t) = \frac{P_f(X,t) - P_f(X,t - \Delta t)}{(1 - P_f(X,t - \Delta t))} \tag{16}$$

$$\Delta\beta(X,t) = -\Phi^{-1}(\Delta P_f(X,t)) \tag{17}$$

In the current work, we consider Δt to be equal to one year and thus, the parameters $\Delta P_f(X,t)$ and $\Delta\beta(X,t)$ correspond to the annual probability of failure and annual reliability index and will be referred to as such in the continuing.

It must be noted that the Frandsen and IEC turbulence models together with partial safety factors are intended for semi-deterministic design and not for probabilistic design and reliability analysis. However, since the partial safety factors are calibrated based on achieving certain reliability level (to which we are also setting the values for) at the end of the design lifetime, the results are comparable. Such comparisons are presented in the next section.

3 Results and discussions

We validate the model of the turbine before performing the study (see Appendix for validation results). The current section presents the results in three parts: Turbulence comparison (Sect. 3.1), fatigue load comparison (Sect. 3.2), and fatigue reliability comparison (Sect. 3.3). The reliability assessment also includes the sensitivity of the reliability level to different random inputs at the target extended life (30 years) in all approaches. Finally, we present the overall discussions on the results in Sect. 3.4.

3.1 Comparison of turbulence levels

Figure 2 presents the comparison between site-specific turbulence based on SCADA data, the Frandsen model, and the IEC design class in different wind direction bins. The plot of each direction bin only includes the mean wind speed bins in which there are enough available data to cover the comparison (more than 20 points). The Whisker box plots in Fig. 2 contain the data from 25% quantile up to 75% quantile, and the red 'plus signs' account for data in the high and low tails and possible outliers.

The scatter of the turbulence versus the corresponding 10-minute DEL measurements in different direction bins are provided in the appendix (see Fig. C2 for precise observation of the placing of the high turbulence points related to the cluster of data). If we consider no outlier in turbulence measurements and approve the data as they are, according to Fig. 2 in the wind bin 1 (free stream condition), the Frandsen model and the IEC design level turbulence underestimate the higher tail of the site turbulence in low mean wind speeds while overestimating it in high mean wind speeds (over the rated speed). In addition, the Frandsen model estimations are higher than design in high mean wind speeds while being the same as IEC representative value in low mean wind speeds. Emeis (2014) claims the same results for the case of design-level turbulence. This trend remains the same almost in all other wind direction bins. Direction bins 2 and 4 include very high wake effects and high turbulence levels and show less conservative assumptions by the IEC class and the Frandsen model in even high mean wind speeds. Figure 2 reveals that in some cases, the Frandsen model does not produce much higher turbulence compared to the IEC design representative turbulence for the class. In the following section, we investigate the differences in terms of fatigue loads and fatigue reliability as more accurate parameters to estimate the lifetime extension based on each turbulence estimation approach.

3.2 $DEL_{lifetime}$ distributions

As shown in Eq. 14, finding the distribution of $log(DEL_{lifetime})$ is a necessity for estimating the probability of failure. The current section presents the distribution of $DEL_{lifetime}$ and $log(DEL_{lifetime})$ based on measurement data (DEL_{10-min}).
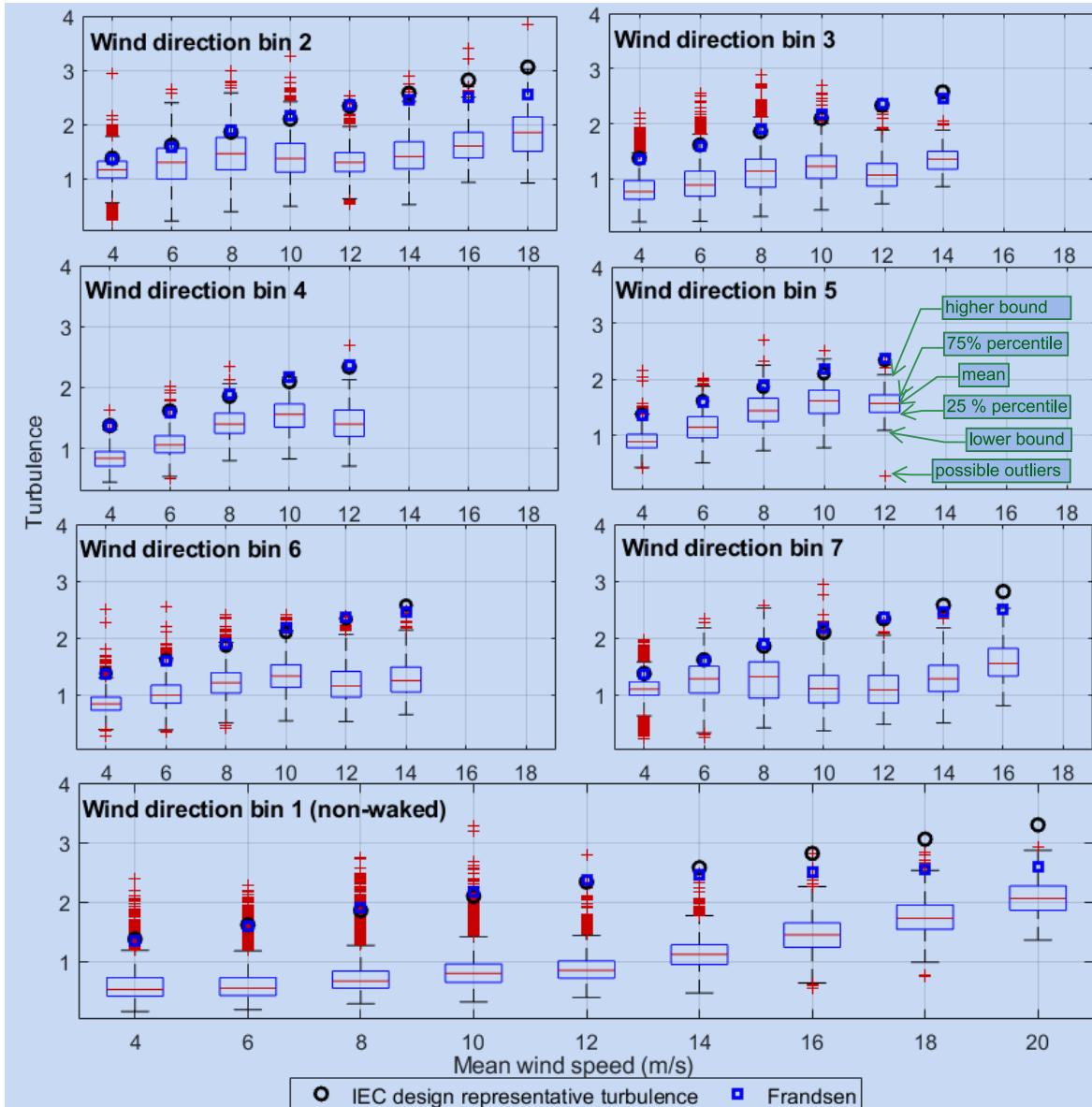
Figure 2. The enhanced turbulence based on Frandsen estimation (blue squares) compared with IEC design representative turbulence (black circles) and the site turbulence measurements (box plots)

First, we observe the empirical probability distribution of the 10-minute DEL measurements, from which we evaluate $DEL_{lifetime}$
365 realizations. Fig. 3 shows the empirical probability density of the 10-minute damage equivalent flapwise moment from measurement data.
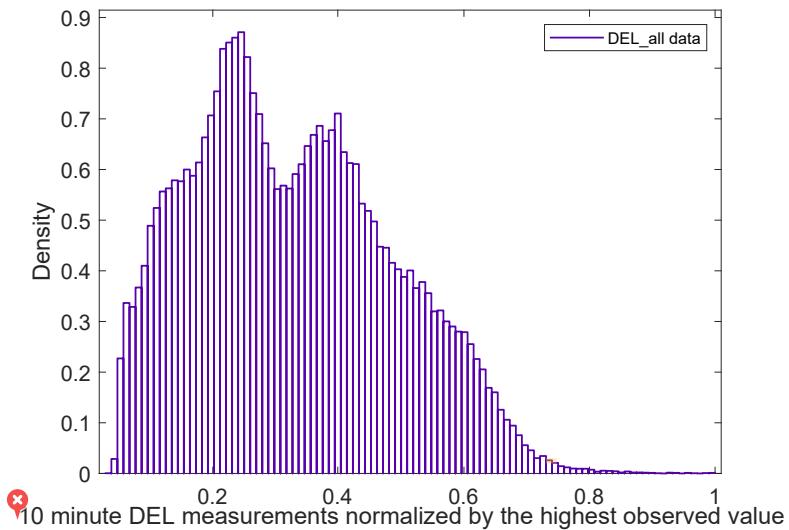
Figure 3. Empirical probability density of the 10-minute DEL measurements in all mean wind speed directions combined

As Fig. 3 reveals, the distribution of the 10-minute DEL data is multi-modal and cannot be represented fully by uni-modal distributions. The multi-modality of the DEL can be a result of having both stratified and un-stratified winds during the observation time, as the same behavior can be seen in each wind direction bin (see Fig. C3 in the appendix). We investigate the mixture of two or three Gamma distributions as well as a mixture of two or three Gaussian distributions as multimodal distributions have shown good candidacy for modelling of fatigue loads (see Mozafari et al. (2023a)). Among all, the mixture of two Gamma distributions appears to be the best fit to describe the statistical behavior of the 10-minute damage equivalent flapwise moments in the case study wind turbine's blade root (in all direction bins combined). Fig. 4 shows this fit on the empirical CDF of data.

As Fig. 4 presents, the Gamma mixture model fits the data well with fair accuracy in the higher tail. We use the probability of exceedance from this model and follow the steps presented in 2.4.3, to find the return load corresponding to 30 years. We use Eq. 10 and Eq. 11 to extrapolate the distribution to a 30-year return load. The slow growth of the tail from year 5 (corresponding to the probability of the largest data observed) to 30 years shows that the distribution is fairly converged, and a five-year return period is enough for the main assumption in Sect. 2.4.3 to hold. Continuing the procedure with bootstrapping as outlined in section 2.4.3, the realization of $DEL_{lifetime}$ in different years is shown in Fig. 5.

As shown in Fig. 5, the mean value of the realizations converges as the standard deviation decreases. This complies with our expectation according to the law of large numbers: The mean converges to the 'true' expected value of $DEL_{lifetime}$ as we gather more observations through the years. The change in the standard deviation with a slight change in the mean value allows for the assumption of non-linear damage accumulation through time (variable DEL through time). We use the converged distribution of $DEL_{lifetime}$ for the estimation of the annual reliability index.
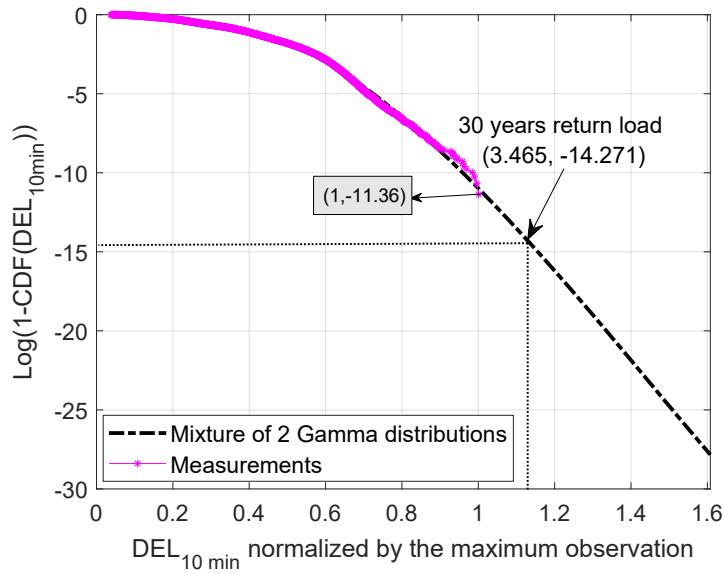
Figure 4. Probability of the exceedance of the DEL based on empirical cumulative distribution function (purple stars) and based on best distribution fit to the data (black dashed line)
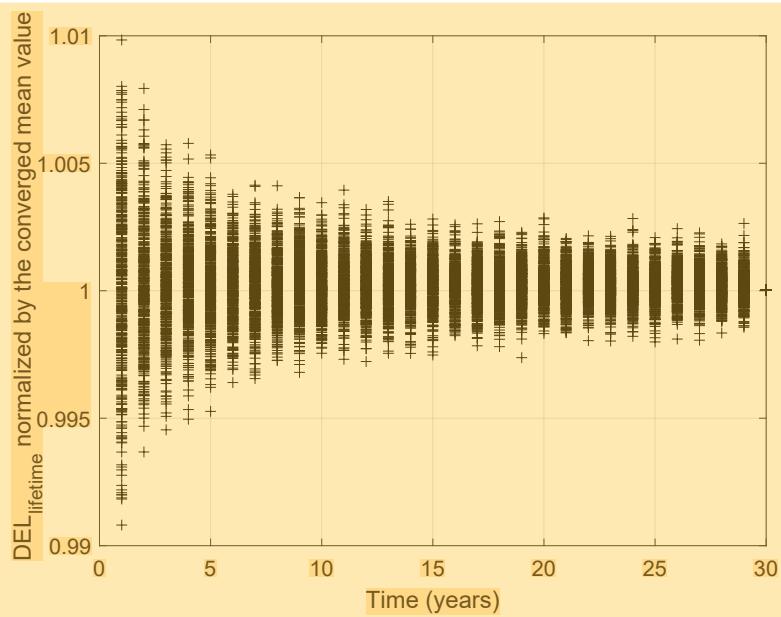
Figure 5. The realizations of $DEL_{lifetime}$ generated via bootstrapping of available 10-minute DEL estimates through years

Fig. 6 presents the PDF of $DEL_{lifetime}$ in two different turbulence scenarios of the IEC 61400-1 representative design value and the Frandsen estimation using bootstrapped data among simulations. The uncertainty of $log(DEL_{lifetime})$ in the site is modelled by a frequentist approach (Maximum likelihood) based on observations in the measurements and includes all sources of uncertainty. However, in the case of the other two approaches, the uncertainty of this parameter is assessed based on bootstrapping and thus, it only includes epistemic uncertainty. The data in Fig. 6 are normalized by the converged mean of $DEL_{lifetime}$ obtained above using site measurements.
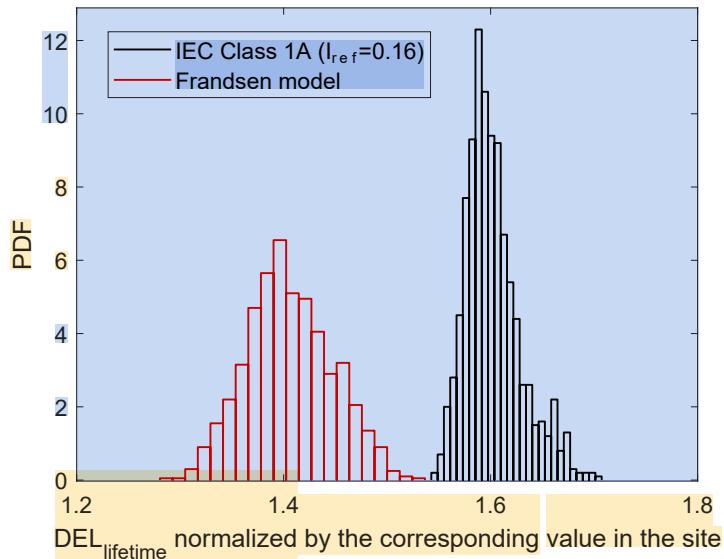
Figure 6. PDF of $DEL_{lifetime}$ in two different scenarios of the IEC standard for design and site-suitability check (based on the Frandsen model) normalized by the mean $DEL_{lifetime}$ estimation based on site's measurements

As Fig. 6 reveals, the estimation of the $DEL_{lifetime}$ based on the representative turbulence for design and the Frandsen estimation are conservative compared to the site-specific assessment based on measurements. The Frandsen model, in this case, leads to respectively less conservative fatigue loads than design-based approach as expected. In addition, the DEL realizations based on the Frandsen model are more spread, showing a higher variability. In the following section, we use the $DEL_{lifetime}$ distribution for assessing the fatigue reliability at the end of the design service life and the possible extended life in different scenarios.

3.3   Reliability and importance ranks

As the model is generic and the material properties are not defined accurately, we assess the lifetime extension after calibrating the material's mean strength. The calibration is made such that we get the target annual reliability index level for a moderate consequence of the failure of a structural component (equal to 3.3) IEC 61400-1 (2019) at the end of design life (25 years).

Fig. 7 presents the annual reliability index for 35 years in all case scenarios based on the calibrated material properties (mean value of strength (K) is multiplied by a factor).
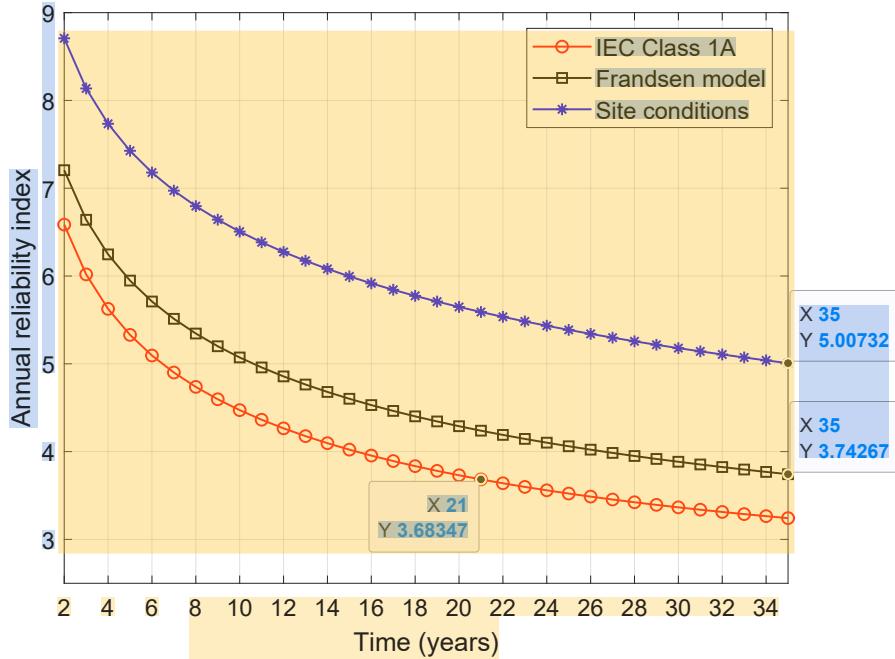
Figure 7. Annual reliability of the case study wind turbine in two scenarios of using Frandsen model (black square) and site load measurements with (blue) versus the IEC design class (red circle)

The difference in the annual reliability levels in different scenarios in Fig. 7 is due to the difference in the turbulence, observed in Sect. 3.1. The reliability of 3.7 at year 35 for the Frandsen model means there is a possibility of a lifetime extension of up to 10 years for the turbine under study when using this model. Using the site data, this level is reached in more years, showing the conservative results from the Frandsen model. The fast drop in the design-based annual reliability in Fig. 7 represents the high mean value of the design DEL compared to the Frandsen model and site. The high difference between the reliability in the two scenarios is due to the high fatigue exponent of the composite increasing the effect of the mean of fatigue loads on the reliability.

Table 4 shows the importance rank of the random variables in the limit state function (see Eq. 14) based on FORM analysis. As Table 4 reveals, the relative importance of the load is low in all three scenarios. The relative importance of the fatigue load is higher in the case of the Frandsen model because of the high coefficient of variation of the DEL in this case. Its sensitivity to loads is almost zero when it comes to the site-specific lifetime DEL. The effects of the uncertainty in the material properties are the highest in all cases because of the very high coefficient of variation. In the site assessment, the reliability is highly sensitive firstly to the material uncertainty and secondly to the damage accumulation rule.

Table 4. The sensitivity of the reliability to different random variables (%) based on three approaches at year 30

Random variables / Assessment basis	Frandsen model	IEC design-level	Site measurements
$log(\Delta)$	38.29	41.70	44.46
$log(K)$	47.84	52.09	55.54
$log(DEL_{lifetime})$	13.87	6.21	7.62×10^{-3}

3.4 Discussion

The data show the conservative estimations of turbulence based on the Frandsen model in high mean wind speeds and, thus, in the overall DEL estimations when considering the blade's flapwise bending moments. The reliability assessments show the possibility of a lifetime extension for more than 35 years while maintaining safety margins.

The very low sensitivity of the reliability to the fatigue loads in the case of site-specific assessment is due to the relatively low coefficient of variation of this variable compared to material strength and Miner's rule. This shows the robustness of $DEL_{lifetime}$ as an accumulated/averaged random variable. The results comply well with the results shown in Mozafari et al. (2023b) showing how the accumulation decreases the coefficient of variation of $DEL_{lifetime}$.

There are some limitations and simplifications in the present study that must be considered and improved in future work. As an example, there is a potential difference in the results of the simulation-based approaches if the model was not generic and the simulations were offshore (considering wave loads). The results of the model validation show that the small differences in load can lead to underestimation of the $DEL_{lifetime}$ in simulation-based scenarios and, thus, the remaining service life. This is especially important in the assessment based on Frandesn model as the sensitivity studies show that the reliability of the Frandsen-based approach is sensitive to the loads.

In addition, the results of the current study are performed on the blade flapwise load channel as a case-study. However, all the load channels shall be investigated for lifetime extension estimation. Furthermore, load channels with deterministic behaviour (for example blade edgewise moments) often have lower design margins and thus are the critical components deriving the lifetime extension of the wind turbine. The current study is not focusing on actual lifetime of the turbine and focuses on showing the difference between Frandsen site-suitability assessment and assessments based on measurements when it comes to fatigue reliability. Such comparison is more clear on a turbulence-driven fatigue load like flapwsie bending moment.

Furthermore, It has to be considered that the data with a return period of 5 years are only referring to winter season and thus the tail shape of the distribution might be different if seasonal variability is also included.

Finally, although the turbulence levels from site and the Frandsen estimation are directly compared, the fatigue load results based on the two are derived differently. The former is based on post-processing of strain-gauge data and the later based on aeroelastic simulations. Thus, the possible bias and errors of the turbine model and aeroelastic simulations can affect the DEL and reliability comparison results.

For future studies, we recommend below studies:

1. Performing the same study on the performance of the Frandsen model in deeper locations within the wind farm, as they usually include more intense/complicated wake conditions.

2. Investigating the effects of using ambient wind data (using Frandsen) instead of local on-site measurements of the waked turbulence considering all the load channels (lifetime extension assessment as a whole) and performing offshore simulations.

3. considering other sources of uncertainty in the reliability assessment framework, including the uncertainty due to the range counting methods, uncertainty in simulations, etc.

4. Investigating the reasons behind the multi-modality of the 10-minute DEL distribution.

5. Performing the same study using independent fittings and extrapolations of DEL in each wind bin for higher certainty and accuracy in the assessment.

6. Joining the study with inspection and health-monitoring data coupled with risks and cost analysis to obtain a complete set of tools for decision-making regarding lifetime extension.

4 Conclusions

The objective of this study is to demonstrate the significant benefits of collecting and utilizing load/displacement measurements, which can outweigh the challenges of such assessments by extending the project lifetime of wind turbines. This research compares two different data availability scenarios—one with structural response measurements and one without—after validating the wind turbine model through simulations using site measurements in free stream directions. In addition, the study addresses two common challenges in fatigue reliability assessments. First, it evaluates the performance of the Frandsen model for estimating waked turbulence and corresponding fatigue loads at Lillgrund, a compact wind farm with mixed-wake conditions. Second, it presents a methodology for extrapolating fatigue loads, showcasing an example application using strain gauge measurements in Lillgrund.

The results indicate that the Frandsen model can yield conservative fatigue load estimations at the investigated location despite the compact layout of Lillgrund. Furthermore, using strain-gauge measurements, results in a 33% higher annual reliability index at the end of 35 years compared to assessment based on ambient conditions and the Frandsen model. The study also reveals that reliability at the end of life, and consequently the lifetime extension assessment, is highly sensitive to material

properties. Additionally, the relative importance of load estimates in assessments based on the Frandsen model is greater than in those based on site measurements. Due to the way fatigue reliability decreases very slowly over the late years of project lifetime, the reduction in uncertainty created by measurements at the site can provide the knowledge basis for many additional years of turbine operation within the acceptable reliability target.

The extrapolation approach presented in the current research facilitates the use of digital twins when strain gauge measurements are unavailable for part or all of the turbine's lifespan. The assessment of the Frandsen model in this case study, representing a wind farm with short spacing, contributes valuable insights to ongoing research on the performance of this model in intense and mixed-wake conditions. Moreover, the findings on the robustness of reliability based on the load estimation approach are crucial for incorporating uncertainty into lifetime extension assessments. Above all, the comparison between scenarios with and without load measurement shows the importance of site load measurements in maximizing lifetime extension, as they significantly reduce uncertainty and enable greater extensions.

Appendix

1 Model Validation

490 As mentioned in Sect. 2.3.2, group 3 simulations are for validation of the model. The input of this group is based on site-specific inputs from the non-waked free stream (wind direction bin 1). First, we compare the mean load levels from the measurements in wind bin 1 to the results of the group 3 simulation. Then, we compare the 10-minute DEL evaluations and investigate the differences in $DEL_{lifetime}$ formed via bootstrapping.

Figures A1 and B1 show the comparison of the mean load levels and 10-minute DELs in the measurements versus simulations, respectively.
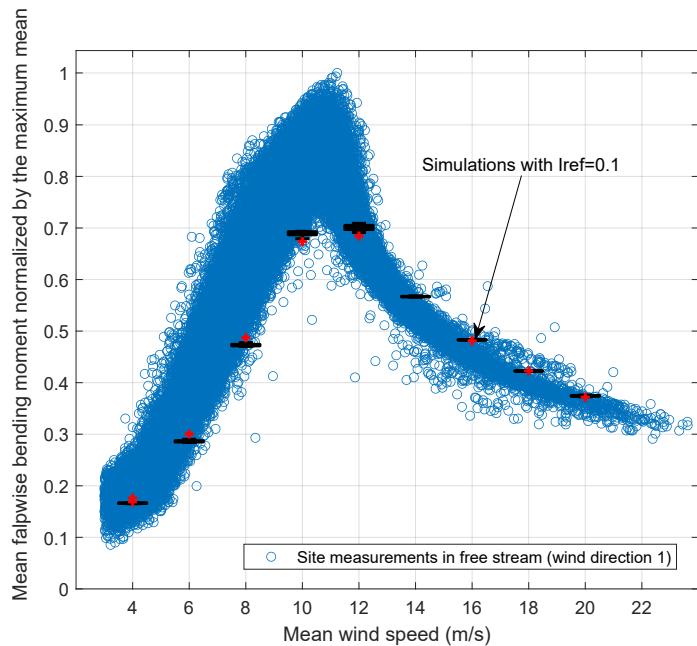
Figure A1. The mean flapwise bending moment in different mean wind speeds in non-waked directions from two sources of measurements (blue circles) and simulations (black boxplots)

495 The data shown in Figure A1 and B1 reveal the high variation in the measured mean load and damage equivalent flapwise moment around rated mean wind speed. The high difference in this area can introduce some errors in the estimations based on simulations (groups 1 and 2) based on dominant (high probability) wind speeds. However, generally, the data shows fair coverage of the site load behaviors.

Fig. C1 represents the power production versus mean wind speed compared with the nominal power curve after filtration.
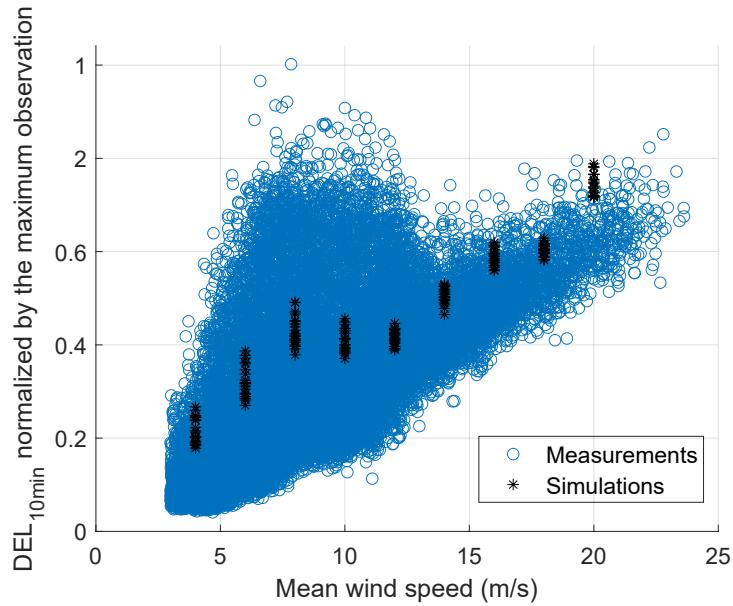
Figure B1. The cluster of 10-minute DEL data in the free stream versus the DEL estimations from simulations in each mean wind speed
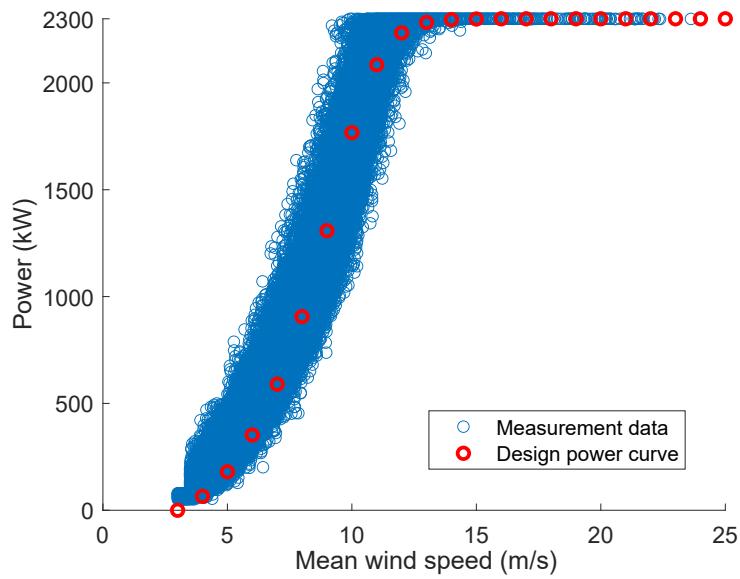
Figure C1. The filtered power production data versus mean wind speed (blue) compared with the nominal power curve (red)

500   Fig. C2 shows that the high tail of turbulence observations mostly belongs to the cluster of data, and the possibility of having a high number of outliers is low. The probability of exceedance of the 10-minute DEL measurements within each wind direc-
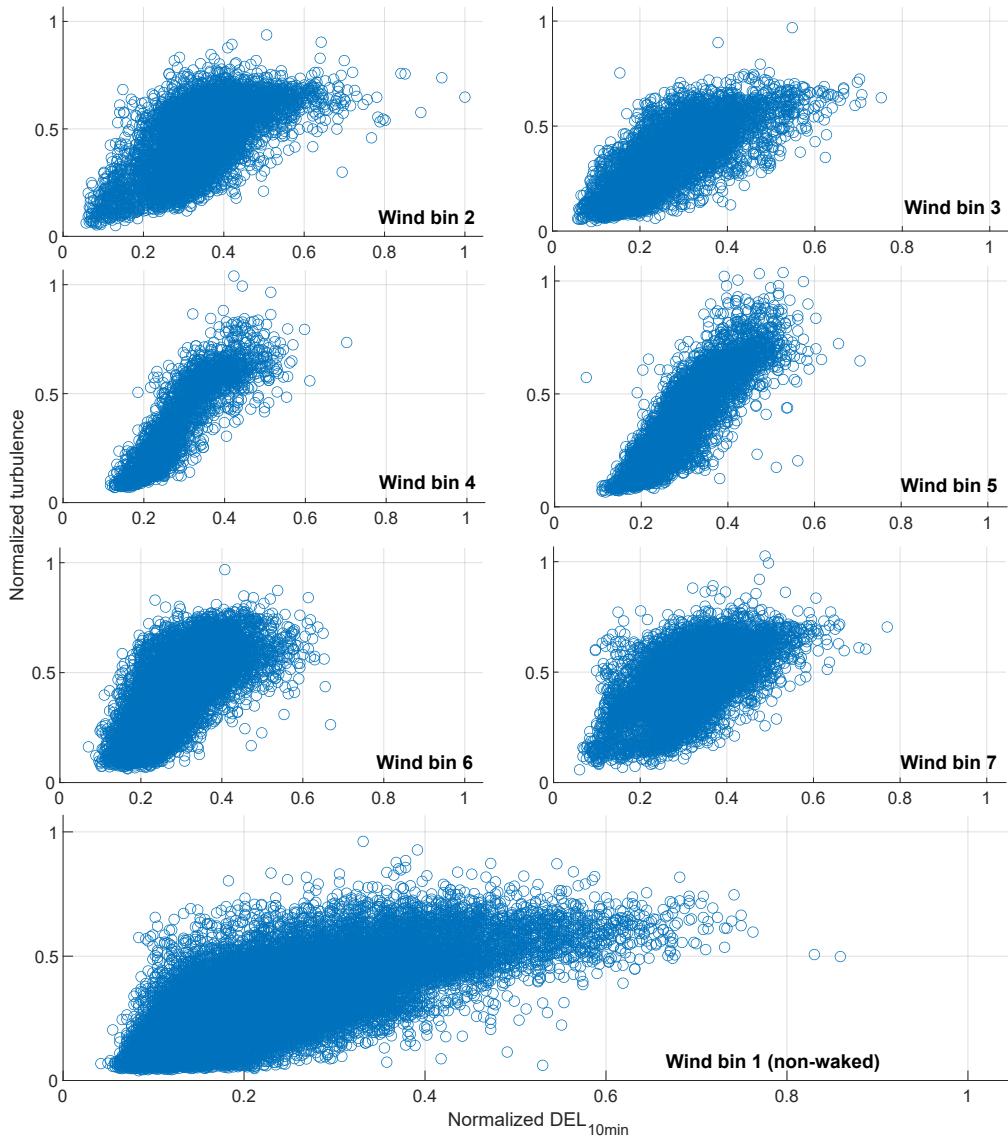
Figure C2. Scatter plot of turbulence data normalized by the highest observations versus corresponding 10-minute DEL observations at the same time in different wind direction bins before filteration

tion bin is shown in Fig. C3 using both the empirical CDF and the best distribution fit to each cluster of data.

Figure C3 shows that the highest DEL observations occur in wind bin 5.
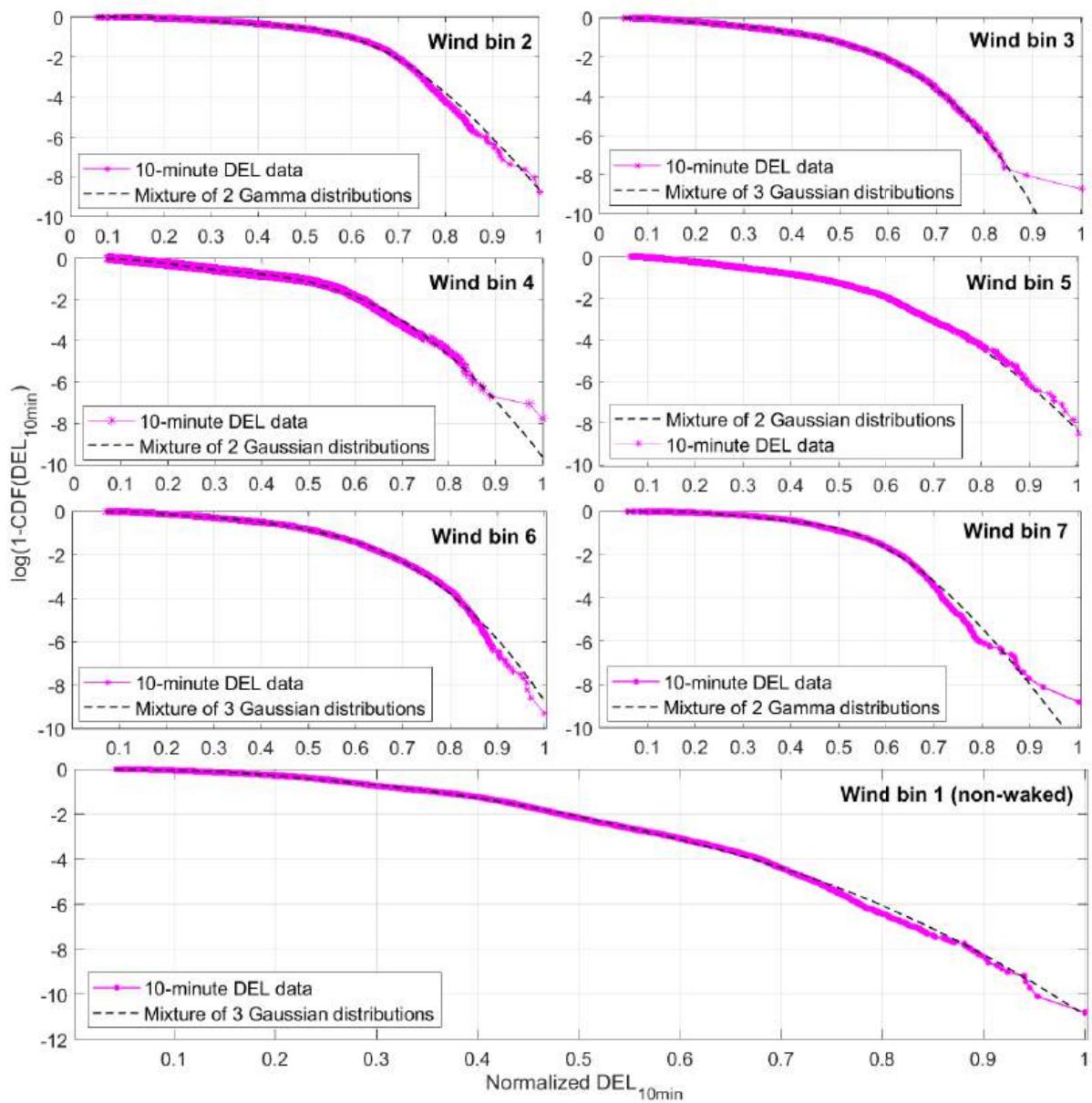
Figure C3. Logarithm of the probability of exceedance of the normalized DEL_{10min} in different wind direction bins in the location of the wind turbine (purple dotted line) and the best distribution fits (black dashed-line)

505   In addition, the data in table A1 reveals that the load fluctuations in the simulations are very small compared to reality. This is partly because of the integration over turbulence distribution (see Mozafari et al. (2024) for details) and partly due to the variability of the environmental condition (see Sect. 3.1). Although the validations show over-estimations of the load and DEL in high mean wind speeds, we proceed with the study using the available HAWC2 model because the difference in the overall DELs shown in Table A1 are less.

Table A1. Statistical parameters of $DEL_{lifetime}$ according to the non-waked aeroelastic simulations using site-specific turbulence and shear exponent versus the same parameters from measurements

Source	Mean DEL normalized by the mean based on measurements	std of the $DEL_{lifetime}$
Site-specific simulations for non-waked area	1	0.014
Measurements for non-waked area	1.04	0.031

510   Different distributions shown in the table below are fitted to the mean wind speed data of the wind turbine. As can be seen, the best fit is the Rayleigh distribution. The maximum likelihood method is used for fitting and the prediction error is measured by Akaike information criterion (AIC).

Table B1. Different distributions fitted using maximum likelihood method to the wind speed measurements

Distribution	Par1	Par2	Par3	Log-Likelihood	AIC
Rayleigh	5.90			-7.23E+05	1.45E+06
Gev	-0.12	3.70	5.47	-7.25E+05	1.45E+06
Normal	7.23	4.17		-7.32E+05	1.46E+06
Gamma	3.00	2.41		-7.40E+05	1.48E+06
Exponential	7.23			-7.65E+05	1.53E+06
Ev	9.39E+00	4.560		-7.68E+05	1.54E+06
Uniform	0.00	2.81E+01		-8.57E+05	1.71E+06

Table C1. The best distribution fits to the $log(DEL_{lifetime})$ in case scenarios of Frandsen turbulence and IEC standard's representative turbulence for free stream

Case	distribution of $log(DEL_{lifetime})$	parameter 1	parameter 2	parameter 3
IEC design based model	Normal	0.2878	0.0143	
Frandsen bsaed model	Gev	-0.2536	0.0298	0.3772

Author contributions. SM, JR, and PV were responsible for the overall conceptualization of the study. SM wrote all the computer codes and performed all the data analysis. SM, PV, and KD were involved in the writing and editing of the manuscript

515 *Competing interests.* At least one of the (co-)authors is a member of the editorial board of Wind Energy Science.

Code and data availability

References

Amiri, A. K., Kazacoks, R., McMillan, D., Feuchtwang, J., and Leithead, W.: Farm-wide assessment of wind turbine lifetime extension using detailed tower model and actual operational history, Journal of Physics: Conference Series, vol. 1222, p. 012034, IOP Publishing, 2019.

520 Argyle, P., Watson, S., Montavon, C., Jones, I., and Smith, M.: Modelling turbulence intensity within a large offshore wind farm, Wind425 Energy, 21, 1329–1343, 2018.

Basquin, O.: The Exponential Law of Endurance Tests, ASTM, p. 625, 1910.

Bayo, R. T. and Parro, G.: Site suitability assessment with dynamic wake meandering model. A certification point of view, Energy Procedia, 76, 177–186, 2015.

525 Bergström, H.: Meteorological Conditions at Lillgrund, The Swedish Energy Agency, 2009.

Commission, G. I. E.: IEC 61400-1, Wind turbine generator systems – Part 1: Safety requirements, 3rd edition, Proceedings of the IEC, pp. 61 400–3, 2005.

Commission, G. I. E.: IEC 61400-1, Wind turbine generator systems – Part 1: Safety requirements, 4th edition, Proceedings of the IEC, pp. 61 400–4, 2019.

530 Dahlberg, J.: Assessment of the Lillgrund Windfarm. 6-1 LG Pilot Report, 2009.

de Oliveira JT, editor. Statistical extremes and applications. Springer Science and Business Media; 2013 Apr 17.

Dimitrov, N. and Natarajan, A.: From SCADA to lifetime assessment and performance optimization: how to use models and machine learning to extract useful insights from limited data, Journal of Physics: Conference Series, vol. 1222, p. 012032, IOP Publishing, 2019.

Dimitrov, N., Natarajan, A.: Probabilistic framework to quantify the reliability levels of wind turbine structures under enhanced control

535 methods Deliverable D2.5, 2020.

ISO, I. "2394." General Principles on Reliability for Structures.—1994.—50p, 2015.

Emeis, S.: Current issues in wind energy meteorology, Meteorological Applications, 21, 803–819, 2014.

Endo, T., Mitsunaga, K., and Nakagawa, H.: Fatigue of metals subjected to varying stress-prediction of fatigue lives, Preliminary Proceedings of the Chugoku-Shikoku District Meeting, pp. 41–44, The Japan Society of Mechanical Engineers, 1967.

540 Faber, M. H.: Statistics and probability theory: in pursuit of engineering decision support, Springer Science and Business Media, Vol. 18, London, 2012.

Fraisse, A. and Brøndsted, P.: Compression fatigue of Wind Turbine Blade composites materials and damage mechanisms, Proceedings of the 21st International Conference on Composite Materials (ICCM-21), Xi'an, China, pp. 20–25, 2017.

Frandsen, S.: Turbulence and turbulence generated loading in wind turbine clusters, Risø report R-1188, 2007.

545 Frandsen, S. T. and Madsen, P. H.: Spatially average of turbulence intensity inside large wind turbine arrays, European seminar offshore wind energy in Mediterranean and other European seas, pp. 97–106, Univ. of Naples, 2003.

Natarajan A, Dimitrov NK, Peter DR, Bergami L, Madsen J, Olesen NA, Krogh T, Nielsen JS, Sørensen JD, Pedersen M, Ohlsen G.: Demonstration of requirements for life extension of wind turbines beyond their design life, 2020.

Hübler, C., Weijtjens, W., Rolfes, R., and Devriendt, C.: Reliability analysis of fatigue damage extrapolations of wind turbines using offshore

550 strain measurements, Journal of Physics: Conference Series, vol. 1037, p. 032035, IOP Publishing, 2018.

Kim, S.-H., Shin, H.-K., Joo, Y.-C., and Kim, K.-H.: A study of the wake effects on the wind characteristics and fatigue loads for the turbines in a wind farm, Renewable Energy, 74, 536–543, 2015.

Larsen, T. J. and Hansen, A. M.: How 2 HAWC2, the user's manual, target, 2, 2007.

Le, X. and Peterson, M.: A method for fatigue-based reliability when the loading of a component is unknown, International Journal of Fatigue, 21, 603–610, 1999.

Lee, S., Churchfield, M., Moriarty, P., Jonkman, J., and Michalakes, J.: A numerical study of atmospheric and wake turbulence impacts on wind turbine fatigue loadings, Journal of Solar Energy Engineering, 135, 2013.

Liew J, Göçmen T, Lio AW, Larsen GC. Extending the dynamic wake meandering model in HAWC2Farm: a comparison with field measurements at the Lillgrund wind farm. Wind Energy Science. 2023 Sep. 8;8(9):1387-402.

Ling, Y., Shantz, C., Mahadevan, S., and Sankararaman, S.: Stochastic prediction of fatigue loading using real-time monitoring data, International Journal of Fatigue, 33, 868–879, 2011.

Mann, J.: Wind field simulation, Probabilistic Engineering Mechanics, 13(4), pp.269-282, 1998.

Megavind: Strategy for Extending the Useful Lifetime of a Wind Turbine, Tech. Rep., 2016.

Mikkelsen, L. P.: The fatigue damage evolution in the load-carrying composite laminates of wind turbine blades, Fatigue Life Prediction of Composites and Composite Structures, pp. 569–603, Elsevier, 2020.

Miner, M. A.: Cumulative damage in fatigue, 1945.

Montavon, C., Jones, I., Staples, C., Strachan, C., and Gutierrez, I.: Practical issues in the use of CFD for modeling wind farms, Proc European Wind Energy Conference, 2009.

Mozafari, S., Dykes, K., Marie Rinker, J., and Veers, P. S.: Extrapolation of the rainflow-counted load ranges for fatigue assessment of the wind turbine's blades, AIAA SciTech 2023 Forum, p. 1541, 2023.

Mozafari, S., Dykes, K., Rinker, J. M., and Veers, P.: Effects of finite sampling on fatigue damage estimation of wind turbine components: A statistical study, Wind Engineering, p. 0309524X231163825, 2023.

Mozafari S, Veers P, Rinker J, Dykes K.: Sensitivity analysis of fatigue reliability in wind turbines: effects of design turbulence and the Wöhler exponent. Wind Energy Science, 9(4), pp.799-820, 2024.

Natarajan, A.: Damage equivalent load synthesis and stochastic extrapolation for fatigue life validation, Wind Energy Science, 7, 1171–1181, 2022.

Palmgren, A.: Die lebensdauer von kugellargern, Zeitshrift des Vereines Duetsher Ingenieure, 68, 339, 1924.

Toft, H. S. and Sørensen, J. D.: Reliability-based design of wind turbine blades, Structural Safety, 33, 333–342, 2011.

Toft, H. S., Svenningsen, L., Sørensen, J. D., Moser, W., and Thøgersen, M. L.: Uncertainty in wind climate parameters and their influence on wind turbine fatigue loads, Renewable Energy, 90, 352–361, 2016.

Vitulli, J., Larsen, G. C., Pedersen, M., Ott, S., and Friis-Møller, M.: Optimal open-loop wind farm control, Journal of Physics: Conference Series, vol. 1256, p. 012027, IOP Publishing, 2019.

Yan BW, Li QS, Chan PW, He YC, Shu ZR. Characterising wind shear exponents in the offshore area using Lidar measurements. Applied Ocean Research. 2022 Oct 1;127:103293.

Ziegler, L. and Muskulus, M.: Fatigue reassessment for lifetime extension of offshore wind monopile substructures, Journal of Physics: Conference series, vol. 753, p. 092010, IOP Publishing, 2016.